Marine Chemistry 246 (2022) 104176

Contents lists available at ScienceDirect

Marine Chemistry

journal homepage: www.elsevier.com/locate/marchem

Cable bacteria activity and impacts in Fe and Mn depleted carbonate sediments

Hang Yin [a], Josephine Y. Aller [a], Bradley T. Furman [b], Robert C. Aller [a,*], Qingzhi Zhu [a,*]

[a] School of Marine and Atmospheric Sciences, Stony Brook University, Stony Brook, NY 11794-5000, USA
[b] Florida Fish and Wildlife Conservation Commission, Fish and Wildlife Research Institute, St. Petersburg, FL 33701, USA

ARTICLE INFO

Keywords:
Cable bacteria
Electrogenic sulfide oxidation
Carbonate sediment
Redox cycling

ABSTRACT

The metabolic activities of cable bacteria enable the oxidation of sulfide to sulfate in anoxic sediment at depth through long distance electron transport coupled to the reductions of O_2 and NO_3^-/NO_2^- in surface sediment. The spatial separation of oxidation and reduction half reactions requires modification of diagenetic models that assume electron donors and acceptors are coupled with each other locally within sedimentary deposits. In this study, we show that cable bacteria can become established and remain metabolically active in sulfidic, but Fe, Mn, and solid phase sulfide-depleted, carbonate muds from Florida Bay, USA. Sediment surface pH maxima reflecting electrogenic metabolism developed between 1 and 3 weeks in sediment incubated in laboratory microcosms with oxic overlying water. Cable filament cell abundances varied over time, with the increase initially focused within the subsurface, but by the end of experiments, cell abundances increased both in subsurface and oxic surface sediment. The development of cable bacteria activity in carbonate muds demonstrates that long-distance electron transport metabolism can utilize subsurface dissolved sulfide (e.g., H_2S) as a sole reductant source for sustained periods without transition to Fe-sulfide and apparently without formation of an intermediate suboxic region associated with Fe and Mn cycling. H_2S consumption occurs initially within the O_2-NO_3^- rich oxic – suboxic zone and transitions to a dominant, but not exclusive, subsurface cable bacteria anodic zone. Once established, cable bacteria significantly altered sediment carbonate cycling. Thermodynamic calculations demonstrated that aragonite and hi-Mg-calcites were supersaturated ($\Omega \sim 2.0$–3.2) in the surface sediment layer (< 0.25 cm depth) and were undersaturated ($\Omega \sim 0.2$) in the anodic zone (1–2 cm depth). Hi-Mg-calcites and aragonite likely precipitated in the surface sediment and dissolved in the anodic region, the dissolution confirmed by elevated porewater Ca^{2+}, Mg^{2+} concentrations. P cycling was coupled to remineralization of organic matter, carbonate mineral cycling, and apparently intracellular accumulation of polyphosphates. Thus, cable bacteria may play an important role in the acquisition of P by seagrasses in carbonate deposits where P is otherwise limited by irreversible adsorption and authigenic mineral precipitation.

1. Introduction

Until recently, models of sedimentary biogeochemical cycling have been based on the concept that oxidation–reduction reactions necessarily proceed through a regular succession of dominant oxidant utilization (O_2, NO_3^-, Mn^{4+}/Mn^{3+}, Fe^{3+}, SO_4^{2-}, CO_2) and associated local transport (e.g., diffusion) of intermediates during the aerobic/anaerobic remineralization of organic matter (Froelich et al., 1979). Since 2010, the capacity for long distance electron transport by bacteria, subsequently termed cable bacteria, has been recognized as an alternative reaction mode by which redox half reactions can be spatially separated but coupled through multi-cellular, electron conducting filaments (Meysman, 2018; Nielsen and Risgaard-Petersen, 2015; Nielsen et al., 2010; Pfeffer et al., 2012). Nonlocal, electron transport from the sulfidic zone to the oxic zone explained both the spatial separation of oxygen reduction and sulfide oxidation, and the presence of pH maxima at the sediment surface and pH minima at depth (Marzocchi et al., 2014; Nielsen et al., 2010). For the location-specific cells in the cable bacteria filament, those in the sediment oxic zone perform oxygen reduction while those in the anoxic zone perform sulfide oxidation, and according

* Corresponding authors.
E-mail addresses: josephine.aller@stonybrook.edu (J.Y. Aller), Brad.Furman@myfwc.com (B.T. Furman), robert.aller@stonybrook.edu (R.C. Aller), qing.zhu@stonybrook.edu (Q. Zhu).

https://doi.org/10.1016/j.marchem.2022.104176
Received 31 March 2022; Received in revised form 4 October 2022; Accepted 5 October 2022
Available online 11 October 2022

to Geerlings et al. (2020) and Geerlings et al. (2021), there is an energy conservation discrepancy between cells. For the cells located in the oxic zone, they only serve as the electron sink, and for the cells in the anoxic layers, they conserve energy. From the geochemical perspective, cathodic oxygen reduction ($O_2 + 4e^- + 4H^+ \rightarrow 2H_2O$) consumes protons and generates pH maxima in the oxic surface sediment, and anodic electrogenic sulfide oxidation ($½H_2S + 2H_2O \rightarrow ½SO_4^{2-} + 4e^- + 5H^+$) consumes free sulfide and releases protons in the deeper anoxic sediment.

The contributions of this filamentous group to microbial communities were not recognized in the past, possibly due to the rigid nature of the cell envelope which hampered cell lysis and DNA extraction (Reimers et al., 2017; Trojan et al., 2016). However, the existence and structure of filamentous conductors in marine sediments have now been confirmed by multiple studies (e.g., Pfeffer et al., 2012). Scanning electron microscope images show that the electron conductors are multicellular filamentous bacteria sharing the same outer membrane with evenly spaced ridges running along the entire length of the filament (Cornelissen et al., 2018; Jiang et al., 2018; Malkin et al., 2014; Pfeffer et al., 2012). More recently, the current transported through the intact cable bacteria filaments has been directly measured, demonstrating that cable bacteria conduct electrons over centimeter scales via conductive fibers embedded in the cell envelop (Meysman et al., 2019). The fluorescence in situ hybridization (FISH) probes have confirmed that cable bacteria belong to the family *Desulfobulbaceae,* which also contains sulfate reducing and sulfur disproportionating bacteria (Burdorf et al., 2017; Malkin et al., 2014; Pfeffer et al., 2012). Currently, multiple species of cable bacteria have been identified from both marine and freshwater sediments (Burdorf et al., 2017; Reimers et al., 2017; Trojan et al., 2016; Xu et al., 2021). The broad species diversity of cable bacteria along with their unique metabolism makes studying their potential function in natural environments conceptually intriguing and biogeochemically important.

The characteristic pH distributions in sediment with cable bacteria electrogenic activity have also been largely overlooked due to the low resolution of traditional pH measurement methods and in some cases obscured by bioturbation (Nielsen and Risgaard-Petersen, 2015; Nielsen et al., 2010; Yin et al., 2021a). Nevertheless, since the existence of cable bacteria was confirmed in 2012, their ubiquitous distribution in natural salt marshes, seasonally hypoxic basins, and subtidal coastal sediment environments (Larsen et al., 2015; Malkin et al., 2014), as well as freshwater sediments (Müller et al., 2016; Risgaard-Petersen et al., 2015; Xu et al., 2021), has been demonstrated. When cable bacteria are active, their metabolism must be considered in models of diagenetic reactions and sediment-water exchange processes (Meysman et al., 2015).

Cable bacteria use oxygen as the primary oxidant (Malkin et al., 2014); however, nitrate/nitrite can also act as electron acceptors when oxygen is depleted, although with much slower kinetics (Marzocchi et al., 2014). The direct attachment of cable bacteria to electrodes with varying potentials implies that additional coupled redox reactions other than sulfides, including Fe^{2+}, could be involved in the long distance electron transport reaction (Reimers et al., 2017). The electron donor presently known to be used by cable bacteria is sulfide, either in dissolved (e.g., H_2S) or solid (e.g., FeS) phases after dissolution (Nielsen and Risgaard-Petersen, 2015; Risgaard-Petersen et al., 2012).

The impacts of electrogenic sulfide oxidation on elemental cycling (sulfur, iron, manganese, calcium, phosphorus, trace metals) and solute fluxes have been relatively well studied in lithogenic sediments (Rao et al., 2016; Risgaard-Petersen et al., 2012; Sulu-Gambari et al., 2016a; Sulu-Gambari et al., 2016b; van de Velde et al., 2016). For example, calcium carbonate precipitation and dissolution are promoted in the electrogenic sulfide oxidation cathodic and anodic zones, respectively. Cable bacteria association with Fe cycling is commonly emphasized. As dissolved H_2S is depleted, cable bacteria transition to the use of Fe-sulfides and as a result, typically expand the suboxic reaction zone that is intermediate between the sulfidic and oxic zones (Nielsen and Risgaard-Petersen, 2015). Enhanced Fe-oxide deposition in the surface sediment caused by subsurface electrogenic sulfide oxidation can diminish the sediment phosphorus flux to the water column by forming iron-oxide-bound phosphorus (Sulu-Gambari et al., 2016b). Fe-oxides can also prevent free sulfide release from sediment, serving as a "fire-wall", against coastal bottom water euxinia in seasonally hypoxic basins (Seitaj et al., 2015). In spite of the possible role of redox reactive metals (e.g., Mn and Fe) in the long-distance electron transport and mediation of sulfide dynamics, their interactions with cable bacteria remain unclear, and there may be complex interactions and potential "cryptic" cycling between redox reactive metals and other redox sensitive species (O_2, NO_3^-, SO_4^{2-}, etc.). For example, recent studies suggest that at least in groundwater, a sulfur disproportionation pathway might play a role in electrogenic sulfide oxidation metabolism; especially for the energy conservation of cable bacteria cells located in the suboxic zone, when Fe^{3+} is present and can generate an elemental S intermediate (Müller et al., 2020).

In this study, we examine cable bacteria metabolic activity and growth dynamics using the functional expression of net electrogenic activity revealed by pH patterns, inferred reaction rate distributions, and filamentous cell abundance rather than direct measurement of metabolism or genetic analyses. We demonstrate the potential for substantial cable bacteria activity in Mn- and Fe-depleted carbonate muds from Florida Bay, USA, and document their biogeochemical impacts in the near absence of Mn and Fe. We examine the effects of electrogenic sulfide oxidation on carbonate dissolution and precipitation in surficial carbonate deposits. We suggest that intracellular phosphate accumulation by cable bacteria may be a critical driver of P cycling in carbonate deposits.

2. Materials and methods

2.1. Sediment sampling

Florida Bay is a semi-enclosed embayment (water depth < 3 m) located between the Florida Keys and the Florida Everglades. Water temperature (21–31 °C) and salinity (25–60) fluctuate seasonally due to restricted water exchange with the open ocean, annual precipitation, and freshwater runoff fluctuations (Ginsburg, 1972; Stabenau and Kotun, 2012). The mud banks and shoals are dominated by the seagrass *Thalassia testudinum* (Fourqurean et al., 1992). A network of carbonate mud banks, interbank lakes, and small islands (keys) characterize the Bay (Wanless and Tagett, 1989). Because of high organic matter input, high bottom water temperature, and limited porewater advection, oxygen penetration in the surface sediment is mostly no more than a few millimeters, and dissimilatory sulfate reduction dominates the sedimentary organic matter remineralization (Ku et al., 1999; Rude and Aller, 1991; Walter and Burton, 1990). In the sample collection region, total Fe and Mn contents generally average ~ 0.1–0.14% and 0.002–0.003% respectively (Caccia et al., 2003), with minimal impacts on diagenetic processes (e.g., Ku et al., 1999; Rude and Aller, 1991; Ullman and Aller, 1985; Walter and Burton, 1990). These Fe and Mn contents are substantially lower than typical near shore terrigenous deposits of ~3.6% and ~ 0.072% respectively (Caccia et al., 2003; Thamdrup, 2000).

Florida Bay sediment was hand-collected from the upper ~10 cm of carbonate mudbank deposits in June 2017 (25.03196°N, 80.68085°W, 30 °C), January 2019 (25.116367°N, 80.817970°W, 21 °C) and August 2019 (25.03268°N, 80.68059°W, 31 °C), packed and sealed into plastic bags, and transported to Stony Brook University (Table 1). The bulk sediment was white in color due to the high carbonate content derived from benthic algae, mollusks, and corals (Ginsburg, 1972). During handling, there was a strong odor of hydrogen sulfide, indicative of sulfate reduction, low reactive Fe, and high dissolved sulfide concentrations in sediment porewater.

Table 1
Sample information, storage time and purpose for experiment series I, II and III.

Series ID	Sample time	Longitude (°W)	Latitude (°N)	Storage time	Incubation period (days)	Purpose
I	Jun-17	80.68085	25.03196	1.5 months	27	Test for CB presence
II	Jan-19	80.81797	25.116367	1 month	106	Detailed time series
III	Aug-19	80.68059	25.03268	4 days	48	Colonization controls

2.2. Sediment processing

The overall experimental objectives were to follow the development, or not, of cable bacteria and their possible impacts on carbonate sediment as a function of time. Three time series experiments utilizing microcosms were done for different primary purposes (Table 1). The initial sediment incubations in June 2017, termed series I, were used primarily to determine if cable bacteria were present and to reveal possible expressions of activity. A second set of microcosm incubations in January 2019, termed series II, incorporated more frequent time series sampling and resolution of sulfide distributions. In addition, we followed the responses of electrogenic activity to deoxygenation of overlying water at the end of series II. A third experimental set in August 2019, termed series III, was focused on further confirming reaction patterns revealed in I and II, and manipulating the sediment to better constrain the spatial scaling of sulfide oxidation related to filament distributions (physical barriers to filaments) (Table 1).

Time series chemical compositions in individual microcosms were monitored using planar optodes, extracted porewater, and visible imaging. Bulk sediment for all experiments was initially sieved through a 1-mm pore size nylon screen mesh with no added water followed by manual homogenization with a plastic spatula. Series I sediment was stored with aeration for ~1.5 months, slurried with seawater, and introduced to microcosms for initial observations during incubation. One microcosm was rectangular (20 × 25 × 5 cm (L × H × W)), and fitted with pH and oxygen planar optical sensors pre-installed onto the inner wall surfaces. Two 6 cm diameter glass tubes were filled to a depth of 10 cm to allow for porewater sampling in discrete depth intervals.

Experiment series II sediment was stored in sealed bottles without aeration in the dark at 4 °C for 1 month before use. Sediment was introduced into six cylindrical microcosms and two rectangular microcosms fitted with optical sensors. Microcosms were monitored and sampled serially as described subsequently. The final sampling and termination of series II after 106 days followed a 6 h period of deoxygenation of overlying water that was designed to examine responses of possible electrogenic activity to lack of oxygen.

Series III sediment was sieved and incubated within a few days after collection. Two cylindrical microcosms were prepared by placing Millipore cellulose filter paper (0.2 μm pore size) at 1 or 1.75 cm depth below the sediment surface, to act as physical barriers to filaments and to confirm the response of carbonate cycling relative to active/inactive electrogenic reactivity and to serve as controls (physical inhibition of filaments). pH planar optical sensors (strips) were also installed in the series III cylindrical microcosms.

In each time series incubation, microcosms were overlain with continuously aerated seawater at 22 °C. The overlying seawater was replaced regularly (~ 3-d intervals) with filtered seawater (10 μm pore size filter; salinity ~25) collected from off West Meadow Beach (Long Island Sound, New York, USA).

2.3. Biogeochemical measurements and analytical methods

Microcosms were monitored for pH, O_2, H_2S, and cable bacteria abundance throughout the 1- to 3-month incubation periods to determine the time points of core sectioning. When sampled, the whole rectangular microcosms and cylindrical cores were vertically sectioned (in air; each core processing took <15 min; resolution: 0.25 cm above 2 cm depth; 0.5 cm downwards), centrifuged (3000 rpm, 10 min), and the porewater was filtered (VWR polyethersulfone syringe filters; 0.2 μm pore size) for analyses of Ca^{2+}, Na^{+}, Mg^{2+}, ΣPO_4^{3-} and total alkalinity. For series I incubations, the two cylindrical microcosms were sectioned on day 27 after pH and H_2S optical sensor patterns indicated that evidence for electrogenic reactions had dissipated in the rectangular microcosm. Series II incubation series were sectioned on day 3, 26, 43 (2 cylindrical microcosms each time), and 106 (duplicate rectangular microcosms). On day 106, overlying water anoxia was generated and maintained by continuously purging with a mixture of N_2 and CO_2 gases (CO_2, 0.04%), while keeping the overlying water at a pH of 8 (monitored by a pH electrode). Anoxia was confirmed using an oxygen electrode. 2D pH and H_2S distribution patterns in the box microcosms were imaged using planar optical sensors before and after the anoxic incubation. The concentrations of other solutes (Ca^{2+}, Na^{+}, Mg^{2+}, ΣPO_4^{3-} and total alkalinity) were measured in porewater extracted immediately after the anoxic incubation. Series III incubations were sectioned on day 48.

Porewater alkalinity was measured using the bromophenol blue colorimetric method (Sarazin et al., 1999). Reactive inorganic phosphate ($H_2PO_4^-$, HPO_4^{2-}, PO_4^{3-}; abbreviated as ΣPO_4^{3-}) was determined colorimetrically using molybdenum blue (Murphy and Riley, 1962). NO_2^- and NO_3^- were measured based on the acidic Griess reaction method (LOD < 1 μM) (Miranda et al., 2001). Ca^{2+}, Na^{+}, and Mg^{2+} concentrations were determined using a Horiba JY Ultima 2C ICP-OES Spectrometer.

Samples for examination of the microbial community were collected on day 0, 4, 9, and 27 from the rectangular microcosm in series I, on day 1, 20, 26, 43, and 106 from the rectangular microcosms in series II, and on day 48 from the cylindrical microcosms in series III. In series I and II experiments, 3-ml cutoff plastic syringes were inserted 5 cm vertically at random positions into microcosms. The subcores were subsequently sliced and preserved in 2% formaldehyde (resolution: 0.25 cm until 1 cm depth; 0.5 cm from 1 to 3 cm depth; 1 cm downwards). In series III experiments, bacterial samples were collected during microcosm sectioning. Aliquots of homogenized sediment samples were dried and used to normalize abundances to dry weight (Aller et al., 2019). Cable bacteria filament identity was confirmed by FISH with a *Desulfobulbaceae*-specific oligonucleotide probe (DSB706) (Manz et al., 1992). Cable bacteria filaments were morphologically distinctive (Schauer et al., 2014), and we could also readily identify them using acridine orange (AO) using epifluorescence microscopy. Compared with the FISH method, AO stained samples generally showed longer filament lengths due to less handling, and better precision of cell counts. Additionally, we used AO rather than 4′, 6-diamidino-2-phenylindole (DAPI) for identifying and counting bacteria because it gave better contrast in our natural sediments.

Following the method development with the FISH technique, the lengths of cable bacteria filaments were enumerated primarily from AO stained samples. Abundances were calculated from the summed filament lengths and an average cell size of 2 μm. Sediment subsamples were first diluted 100-fold with 3% saline water and homogenized. AO stained samples were deposited on black GVS polycarbonate track-etched filters (0.2 μm pore size). Cable bacteria filaments were counted within 10 randomly selected fields (1000× magnification; defined by a Whipple reticle) including any that extended beyond the grid field (the same filament only counted once). The inclusion of parts of filaments outside the chosen grid field had the potential to overestimate the cable cell abundance as they sometimes expanded across multiple grid fields. Other filamentous bacteria like *Beggiatoa* can be easily excluded from

erroneous enumeration based on the distinctive cell morphology. No non-filament cells were counted as cable bacteria, although they can apparently occur as isolated, single cells (Müller et al., 2020).

The pH imaging planar optical sensors were made by immobilizing 8-hydroxy-1,3,6- pyrenetrisulfonic acid trisodium salt (HPTS) into a transparent polyester film (Zhu et al., 2006). The responses of the sensor films were captured using a commercially available camera (EOS Rebel T7i), following ratiometric calibration (emission wavelength: 545 nm; excitation wavelengths: 510 nm and 430 nm). pH data reported here are on the NBS scale. Oxygen sensing films were made with platinum tetrakis (pentafluorophenyl) porphyrin (Lee and Okura, 1997). The same camera system was used with an excitation wavelength of 395 nm and an emission wavelength of 650 nm. Oxygen concentrations were calibrated based on the Stern-Volmer relationship (Lee and Okura, 1997) using a two-point calibration: in air saturated seawater (100% air saturation) and in anoxic sediment (0% air saturation). Gas permeable H_2S sensors were made using the diphenylcarbazone-Zn complex (Yin et al., 2017). Both the sample and calibration strip responses were recorded using a flatbed scanner (Canoscan 8400F). Standard solutions were made by adjusting the pH of Na_2S standards below 4 to convert sulfide into dissolved H_2S (> 99.9% conversion). 2D pH, O_2, and H_2S sensor image data were converted to 1D-vertical profiles by horizontally averaging vertically oriented membranes (widths ~0.5 cm). In addition to the optical sensors described above, microelectrodes for pH, O_2, and H_2S (pH, 100 μm tip diameter; O_2 and H_2S, 50 μm tip diameter; Unisense A.S., Denmark) with a manual micromanipulator and a multimeter (PA2000; Unisense A.S., Denmark) were used to resolve vertical profiles of the series II rectangular microcosms on day 1, 6, 16 and 25 for O_2 and H_2S, and on day 2, 19 and 27 for pH. The same standards as optical sensor calibrations were used for microelectrode calibrations.

2.4. Geochemical models

Carbonate speciations were calculated from total alkalinity and pH data using *CO2calc* (Robbins et al., 2010). The thermodynamic equilibrium constants for aragonite and Mg-calcite (5–20 mol% Mg, natural biogenic mineral values) were adopted from Millero (1979) and Morse et al. (2006).

We modeled the production and consumption rates of H_2S (R-H_2S), Ca^{2+} (R- Ca^{2+}), and phosphate (R-ΣPO_4^{3-}) using the program PROFILE (version 1.0) assuming local steady state (Berg et al., 1998). The depth resolution was chosen to correspond to primary geochemical property distributions (e.g., O_2 + NO_3^- oxidant zone) consistent with sampling resolution and to minimize numerical noise. No ionic drift corrections were made due to their small effects on the target reaction rate estimations (below 5% on Ca) and the relatively large errors in modelling the ionic drift terms (Hermans et al., 2021; Malkin et al., 2017). Ion pairs were also not considered. Diffusion coefficients (HS^-, Ca^{2+}, and $H_2PO_4^-$) were corrected for temperature, salinity, and tortuosity using a modified Weissberg model (Boudreau, 1997). The reaction rate units reported here are expressed as μM/d (relative to porewater volume).

We estimated current density associated with electrogenic activity based on R-H_2S. Other workers have used alkalinity reaction balances within the anodic and cathodic zones (e.g., van de Velde et al., 2017). The sulfide consumption rate over the deeper sulfide consumption zone, as calculated in section 3.2, was converted to an equivalent electron flux (R-H_2S × corresponding depth interval), and then to current density through the eq. 1 mA = 1.036×10^{-8} mol e^-/s assuming a $8e^-$ anodic half-reaction.

To estimate the effects of cable bacteria intracellular phosphorus assimilation on porewater phosphate concentration, surface sediment was treated as closed and each individual cable bacteria cell was idealized as a perfect cylinder (OD: 0.6 μm; length: 2 μm). The empirical eq. $DW = 435 \times V^{0.86}$ was used to estimate the individual cell dry weight (Loferer-Krößbacher et al., 1998), where DW is the dry weight (fg) of an individual cell; V is the volume (μm^3) of an individual cell. The cellular carbon content was assumed to be 50% of DW. Based on the previous study, the area of each polyphosphate inclusion comprises 4.2% of the total planar cell area and the P/C ratio of the inclusion is 5.6 times greater than the rest of the cell (Sulu-Gambari et al., 2016b). Instead of using the Redfield P/C ratio assumed by Sulu-Gambari et al. (2016b), we chose the bacteria P/C ratio (0.052 mol/mol) as the cell composition without inclusions (Fagerbakke et al., 1996). The individual cable bacteria cell P/C was calculated as 0.072 mol/mol (assuming 2 inclusions on average per cell; $0.916 \times 0.052 + 2 \times 0.042 \times 5.6 \times 0.052$). The effects of intracellular phosphorus incorporation were calculated from the closed system solid-fluid mass relation:

$$\Delta C_{pw} = \Delta C_{solid}\left(\rho_s \frac{(1-\varphi)}{\varphi}\right)$$

where ΔC_{pw} is the porewater phosphate concentration change (μM); ΔC_{solid} is the intracellular phosphate content (μmol/g), estimated by multiplying individual cell phosphate content (μmol/cell) with sediment cell abundance (cell/g); ρ_s is sediment density (2.6 g/ml); φ is sediment porosity.

3. Results

3.1. Electrogenic sulfide oxidation development

Sediment pH and H_2S dynamics in series I rectangular microcosm showed distinct characteristics of electrogenic sulfide oxidation. A sediment surface pH maximum was evident on day 9 but dissipated on day 27 (Fig. S10 & S11). Electrogenic sulfide consumption was observed throughout incubation but H_2S built up in the subsurface zone after the electrogenic pH fingerprint dissipated, and the depth of detectable H_2S shoaled to around 0.6 cm (Fig. S12).

The dynamics of pH and H_2S distributions were similar in series II but the specific timing differed from series I. For the series II microcosms, pH profiles obtained by both planar optical sensors and microelectrodes demonstrated the development of strong pH maxima in the oxic layer of the surface sediment before day 26–27 (microcosm A, Fig. 1; microcosm B, Fig. S1; microelectrode data, Fig. S2). The pH maximum zone was about 2 mm wide with a maximum value of ~8.5. pH in the underlying anoxic sediment decreased from 7.0 to 6.5 gradually from day 1 to 26 and changed slightly with depth after that. Even though electrogenic sulfide oxidation impacts the penetration depth of O_2, due to the rapid sulfate reduction/sulfide production rates in Florida Bay sediments, O_2 penetration depth was about 2 mm and did not show much variation (i.e., within measurement error, Fig. S3).

H_2S dynamics were also closely related to the development of electrogenic sulfide oxidation in series II microcosms (Fig. 2). After microcosms were set up, H_2S started to build up quickly from day 1 to 20. When electrogenic sulfide oxidation was initiated, as reflected by the pH patterns, sulfide consumption rates increased, and the depths at which H_2S was detectable deepened from 0.5 cm (day 20) to 1–1.4 cm (Figs. 1, 2 & S1). Although not strongly indicated, cable bacteria activity appears to have decreased on day 106 as evidenced by the decreased magnitude of the sediment surface pH maxima (from 8.5 to 8.3, day 87 and 106, respectively) along with a cessation of the H_2S detectable depth in microcosm B (Fig. 2B & S1).

3.2. H_2S consumption

H_2S production and consumption rate patterns estimated in series II using the program PROFILE discriminated different net reaction zones with time (Fig. 1B & S1B). On day 1 in series II, when cable bacteria activity was not developed, H_2S was consumed in the top 3 cm and produced at depth with low rates (−20 and 110 μM/d, respectively) (Fig. 1B). The reaction rates estimated at this initial stage of incubation were partially caused by artifacts when H_2S profiles were measured only

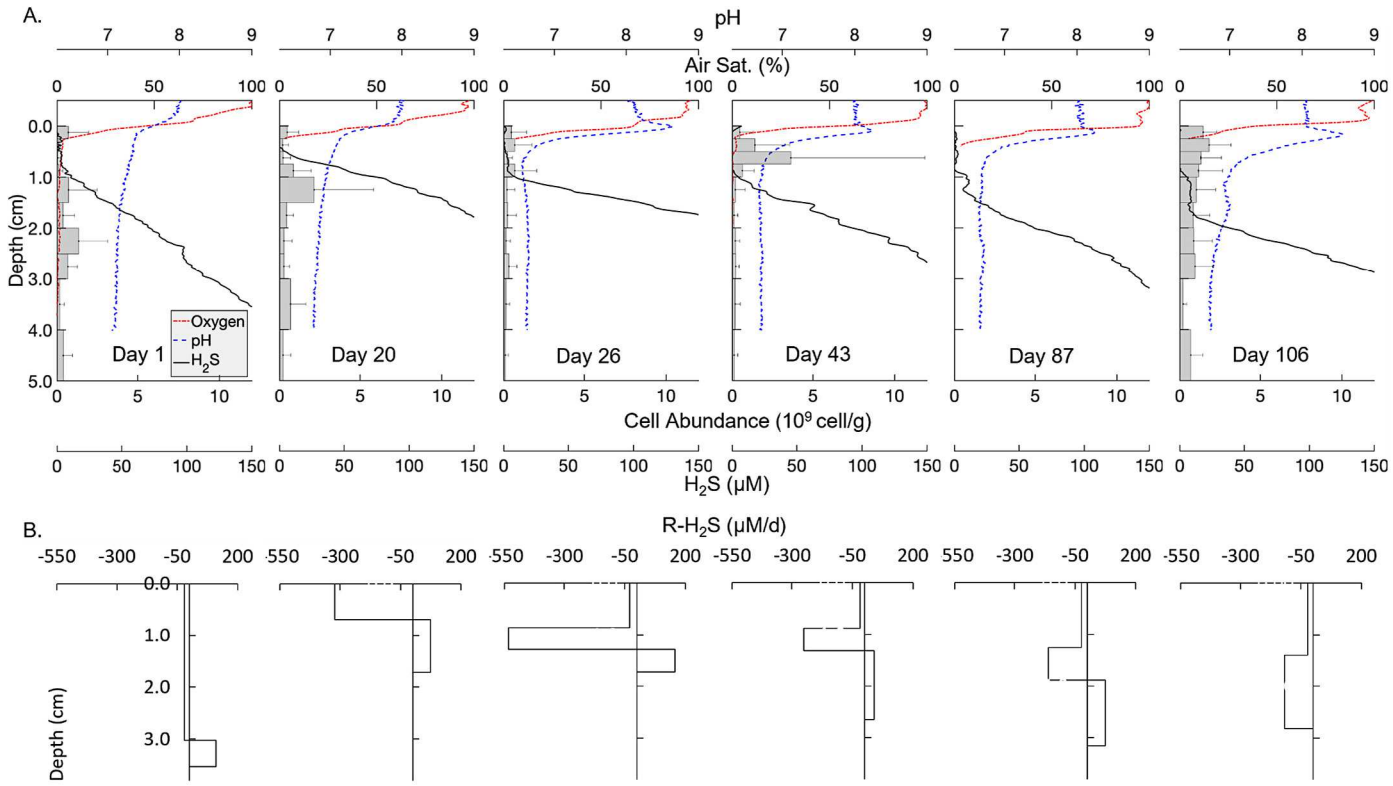

Fig. 1. Distribution of oxygen (red), H_2S (black), pH (blue) and cable bacteria abundances (shaded bar) in series II experiments and the associated H_2S reaction rates (R-H_2S) (duplicate microcosm data in Fig. S1) on day 1, 20, 26, 43, 87, and 106 (no bacteria sample on day 87). A. Sediment surface pH maximum evident after a 3 week incubation. In contrast, pH at depth decreased from 7 to 6.5–6.7 on Day 26. Oxygen penetration depths are ~2 mm and did not change significantly throughout the incubation period (see Fig. S3). The depth of detectable H_2S also became deeper with time. During incubation, an increase in cell abundance was found in the sediment anoxic zone. By day 106, overall more cable bacteria cells were found with a more homogeneous vertical distribution. B. R-H_2S calculated by PROFILE program. A negative rate means H_2S consumption while a positive rate means H_2S production. With the development of cable bacteria activity, the deep consumption zone at depths ≥1 cm gradually became evident, and the upper boundary of the consumption zone deepened with time. Error bars (one side) stand for the standard deviations of bacteria enumeration. (For interpretation of the references to color in this figure legend, the reader is referred to the web version of this article.)

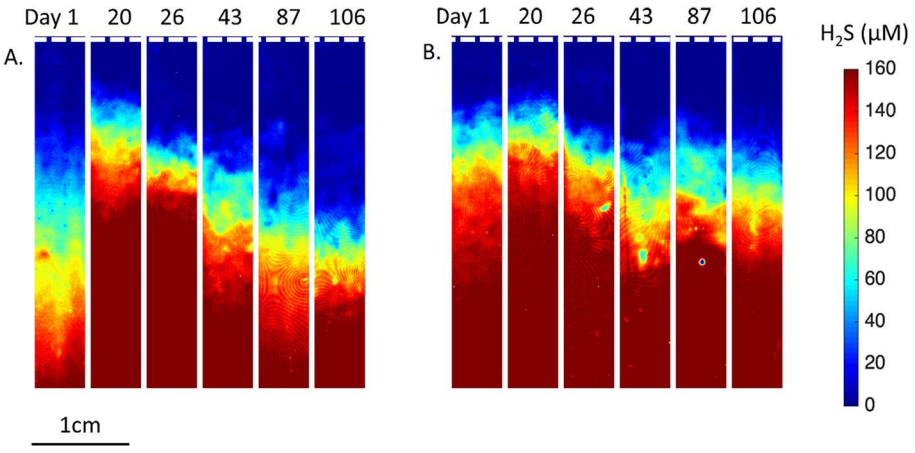

Fig. 2. 2D H_2S distribution dynamics in series II duplicate microcosms (A and B). A. Depths of detectable H_2S (~ 5 μM) decreased from day 1 to day 20 reflecting H_2S build up. From day 20, electrogenic sulfide oxidation caused the detectable depth of H_2S to deepen well below the O_2 penetration zone of a few mm. B. For the duplicate microcosm on the right, H_2S dynamics exhibited a similar trend. However, the depth of minimum detectable H_2S (the electrogenic oxidation front) stopped increasing after day 43 probably caused by the decrease in cable bacteria activity. White dashed lines indicate the sediment-water interface. H_2S dynamics in the deeper sediment are shown in Fig. S4.

one day after the sediment was handled and were still changing rapidly. On day 20, the H_2S net production zone shoaled to a depth of 0.7 cm. When cable bacteria activity first became well-developed on day 26, as indicated by the sediment surface pH elevations, two distinct H_2S reaction zones appeared within the upper 1.3 cm sediment, an upper reaction zone just below the sediment-water interface, overlapped with nondetectable sulfide (Fig. 1A), and a deeper consumption zone below 0.9 cm. The H_2S consumption zones at depth (deep consumption zone) were distinguishable from the upper reaction zones from day 26 to day 106 (Fig. 1B). The upper boundary of the deep H_2S consumption zones also moved downward over time. No H_2S production zones were detected on some of the days (e.g., day 106 for microcosm A) due to the limited scale of H_2S data available (limited by the dynamic range of the analytical method, i.e., the production zone was below 3 cm).

In the other rectangular microcosm of series II (microcosm B; Fig. S1B), the deep H_2S consumption zone was also evident from day 26 to 43 along with cable bacteria activity. However, the consumption rates in the deep zone decreased after day 43 and blended in the shallow

reaction zone. For example, on day 106, only a single consumption zone was distinguishable.

Estimated minimum current density in the series II experiments varied with time and ranged from 3 to 20 mA/m^2, which was the lower end of previously reported values (Table 2) (Nielsen and Risgaard-Petersen, 2015; van de Velde et al., 2017). Current density estimates are minima because only the net consumption rates of H_2S can be calculated from concentration profiles, which also incorporate H_2S production by sulfate reducers. In microcosm B, current density decreased with time from day 26 to 87 and cannot be estimated on day 106 due to the statistically indistinguishable deep sulfide consumption zone rate (see section 4.1 for discussion).

3.3. Cable bacteria distribution dynamics

Cable bacteria filaments were present throughout the top 5 cm in Florida Bay sediments changing in abundance during the microcosm incubation time series (Figs. 1, 3 & S1; Table 2). On day 1 in series II, only short filaments (~3–5 interconnected cells) were found, and filaments were more homogeneously distributed throughout the sediment. From day 20 to 43, during which time sediment surface pH maximum and anodic pH minimum zones were established in the duplicate microcosms, greater numbers of cable bacteria cells were found in the sediment depth between 0.25 and 1.5 cm, at around the same depth of the sediment suboxic zone, while the cell abundance in the sediment surface oxic zone did not change within the counting error (see also Yin et al., 2021b). When cable bacteria activity began to dissipate (presumably in microcosm B on day 106, in series II) or completely disappeared (day 27, in series I), instead of a decline in total standing stock (e.g., cells in the upper 5 cm, Table 1), cable bacteria cell abundances became more homogeneously distributed vertically. Filament abundances increased in the sediment deeper than 1.5 cm as well as in the oxic layer (< 0.25 cm depth), with eventually, more filamentous bacteria cells located in the upper sediment layer (< 0.5 cm depth; Fig. 1A, S1A & S10).

3.4. Carbonate mineral dynamics

Frequent sampling in series II experiments resolved carbonate dynamics associated with cable bacteria development. Porewater Ca^{2+}/Na^+ mol ratios in the surface sediment were about 0.023 (<0.25 cm; overlying water ratio: 0.020) and enriched in the 0.5–1 cm depth with the Ca^{2+}/Na^+ ratios reaching 0.027 on day 26 when the sediment surface pH maxima became well developed (Fig. 4). After day 43, similar Ca^{2+}/Na^+ patterns were observed, but with the Ca^{2+}/Na^+ ratio peaks much broader and higher (Ca^{2+}/Na^+ ratio maximum over 0.031) and at a deeper depth (1–2 cm). Thermodynamic saturation state calculations based on the optical sensor pH, porewater Ca^{2+}/Na^+ and alkalinity data demonstrated that aragonite was supersaturated in the surface layer (Ω = 2–3) and under-saturated at depth, with saturation minima (Ω = 0.2–0.3) centered between 0.5 and 1.5 cm depth. The Ω minima were at the same depth intervals as Ca^{2+}/Na^+ peaks and deep H_2S consumption zones (Fig. 1B & S1B). A white layer of carbonate precipitate was also visible just below the sediment-water interface (1–2 mm depth), consistent with recently formed authigenic carbonate precipitates (Fig. S6). Corresponding to the enrichment of Ca^{2+}, R-Ca^{2+} simulations showed that there was a distinct Ca^{2+} production zone in the top 1–2 cm sediment (1500–3200 μM/d) and a weak consumption/production zone in the deeper sediment (−150–200 μM/d) on day 43 (Fig. 4C). The hypothesized negative R-Ca^{2+} at the sediment surface, indicating precipitation, could not be discriminated due to the coarse resolutions of both sampling and the PROFILE model.

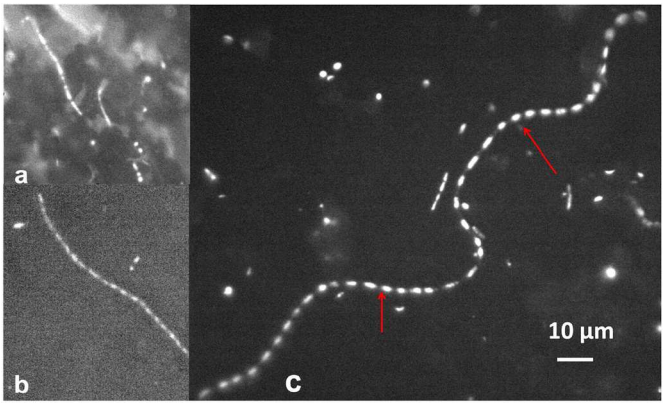

Fig. 3. Images of cable bacteria from series II experiments under an epifluorescence microscope stained with acridine orange. Sediment sample from depths of (a) Day 1: 0.75–1 cm, microcosm B; (b) Day 19: 3–4 cm, microcosm A; (c) Day 106, 0–0.25 cm, microcosm B. Scale bar is the same for all images. Red arrows indicate oval-shaped nucleoid regions found in cable bacteria filament within the sediment oxic layer. (For interpretation of the references to color in this figure legend, the reader is referred to the web version of this article.)

Table 2
Top 5 cm depth-averaged cable bacteria abundance, integrated filament density and current density in series II duplicate microcosm incubations on day 1, 20, 26, 43, 87 and 106.

Time (day)	1	20	26	43	87	106
	depth averaged cable bacteria abundance (10^8cell/g)					
Microcosm A	4.66	5.76	2.47	4.38	N/A	8.29
Microcosm B	5.25	1.97	3.45	6.71	N/A	9.07
	Integrated cable bacteria density (m/cm^2)					
Microcosm A	1460	1810	773	1370	N/A	2600
Microcosm B	1650	616	1080	2100	N/A	2840
	current density (mA/m^2)					
Microcosm A	N/A	N/A	18	9	8	13
Microcosm B	N/A	N/A	15	8	3	N/A

Mg^{2+}/Na^+ ratios were low in the sediment oxic layer (e.g., 0.109–0.110) and increased with depth on day 26 and 43 (Fig. 6). In the anoxic layer, Mg^{2+}/Na^+ did not show an obvious Mg^{2+}/Na^+ enrichment peak after the development of electrogenic reactions on day 26. Thermodynamic calculations indicated that hi-Mg-calcite (5–20 mol% Mg) was supersaturated (Ω = 2–3) in the surface layer and undersaturated at depth with a saturation state minimum (Ω = 0.2–0.3) between 0.5 and 1.5 cm depth on both day 26 and 43 (Fig. 6).

The lower time resolution in series I did not allow for a detailed analysis of Ca^{2+} or Mg^{2+} dynamics as in series II. However, after the electrogenic activity naturally diminished on day 27 for series I (Fig. S14), peaks of Ca^{2+}/Na^+ (reaching 0.027) centered at 2 cm depth were sustained in the duplicate cylindrical microcosms. Similar to the data collected in series II, Mg^{2+}/Na^+ also increased with depth within the electrogenic sulfide oxidation zone without showing an enrichment peak in the anoxic sediment. Thermodynamic calculations indicated that both aragonite and hi-Mg-calcite are supersaturated in the sediment oxic layer with the saturation states Ω = 1.5 and 1.4, respectively, and the saturation state minima (Ω = 0.3) associated with cable bacteria anodic zone reaction were in the 1–1.5 cm depth interval.

In series III, the electrogenic pH fingerprint was absent in cylindrical microcosm a (filter barrier at 1 cm) and evident in cylindrical microcosm b (filter barrier at 1.5–1.75 cm) after 48 days of incubation (Fig. 5). Anoxic sediment Ca^{2+} enrichment was observed only in cylindrical microcosm b but not in microcosm a, consistent with electrogenic pH signals in microcosm b but not in a.

3.5. Phosphate dynamics

Phosphate concentrations increased with depth in all microcosms of

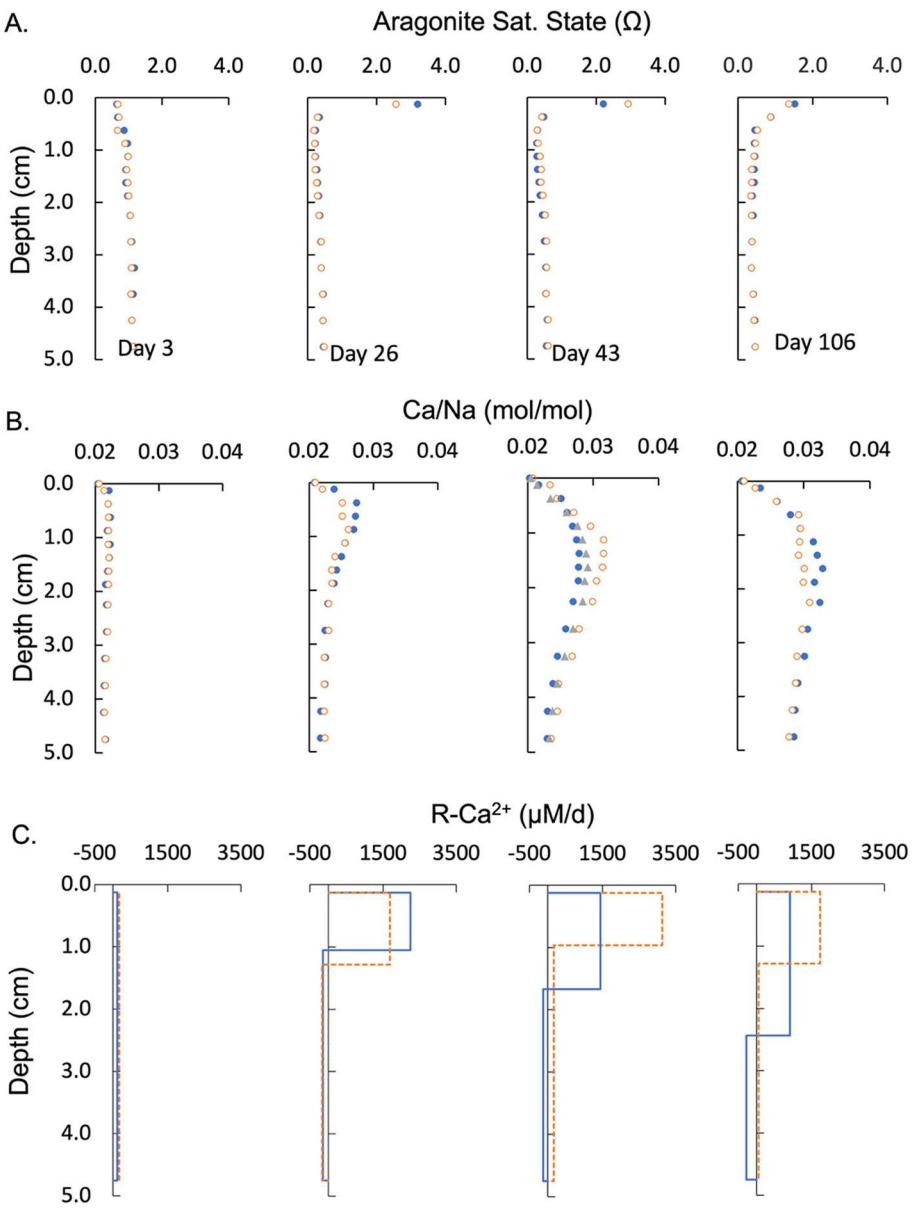

Fig. 4. Aragonite saturation state, Ca^{2+}/Na^{+} distribution dynamics, and the associated Ca^{2+} reaction rates (R- Ca^{2+}) in series II experiments. A. Aragonite saturation state on day 3, 26, 43, and 106. The profile on day 106 was obtained after 6 h with anoxic overlying water. Along with cable bacteria activity, aragonite became super saturated in the surface sediment on day 26 & 43, and a Ω minimum was also evident. After 6 h of overlying water anoxia, aragonite in the sediment surface became less saturated, and the Ω minimum disappeared. B. Ca^{2+}/Na^{+} distribution dynamics. Ca^{2+} was enriched at 0.5–1 cm depth on day 26 suggesting carbonate dissolution. Along with cable bacteria development, Ca^{2+} concentrations in the anodic zone increased and a broader Ca^{2+} enrichment peak developed centered at 1–2 cm on day 43. After 6 h of anoxic incubation on day 106, the Ca^{2+}/Na^{+} peak still persisted in the same depth interval as on day 43. C. R- Ca^{2+} calculated by PROFILE program. Positive R- Ca^{2+} reflecting Ca^{2+} production was simulated in the shallow part of the sediment (depth < 2 cm) while much slower rates of Ca^{2+} production/consumption were observed in the deep part of the sediment. Color coding (blue and orange) shows results from duplicate microcosms. The gray triangles in day 43 profile are the modeled average Ca^{2+}/Na^{+} ratios as it would appear if the production/consumption of Ca^{2+} ceased immediately after anoxic exposure for 6 h and then diffusion was the only process controlling its distribution. (For interpretation of the references to color in this figure legend, the reader is referred to the web version of this article.)

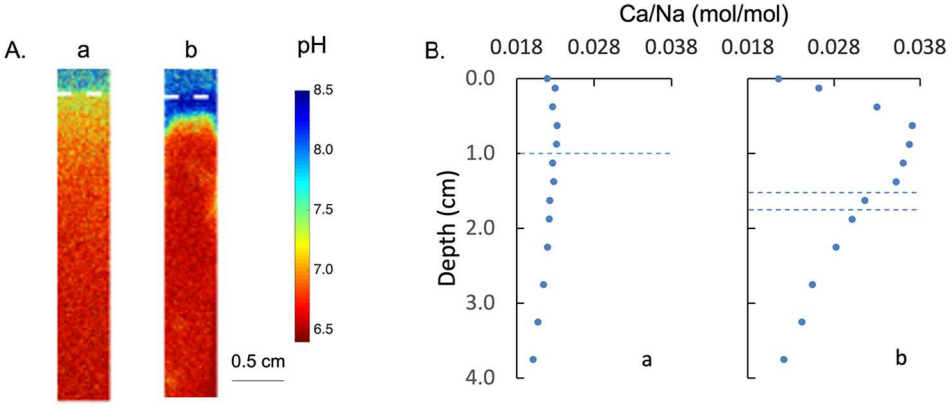

Fig. 5. 2D pH and Ca^{2+}/Na^{+} distributions with filter paper barrier in cylindrical microcosms on day 48 in series III experiments. A. 2D pH distributions. Electrogenic pH fingerprint was evident in microcosm b, where filter paper was found slanted in the 1.5–1.75 cm depth interval, while no signature of electrogenic sulfide oxidation was observed in the control microcosm a where filter paper was placed at 1 cm depth. Horizontal dashed lines indicate the sediment-water interface. B. Ca^{2+}/Na^{+} distributions. A distinct Ca^{2+} enrichment peak centered at 1 cm depth was observed in microcosm a while no such enrichment was observed in microcosm b. Horizontal lines in Ca^{2+}/Na^{+} profiles represent the depths or depth intervals of the retrieved filters.

series II. Within the electrogenic reaction zone (top 2 cm) of carbonate sediments, phosphate concentrations were low (<10 μM), and decreased with time of incubation (Fig. 7A). In series II, a concave-shaped curve was also observed from day 26 in the depth interval of 1–2 cm. Reaction rate calculations showed that there was a phosphate net consumption zone located in the top 1.5–2.5 cm (−0.5 to −2.5 μM/d) underlain by a

net production zone (0.2–1.5 μM/d) (Fig. 7B). The depth intervals of the phosphate consumption zones were consistent with the Ca^{2+} enrichment peaks and the simulated Ca^{2+} production zones (Fig. 4).

3.6. Effect of overlying water O_2 on Ca^{2+}, Mg^{2+}, mineral saturation states, and ΣPO_4^{3-}

After deoxygenating the water overlying cores with a N_2/CO_2 gas mixture for 6 h on day 106 of series II, the sediment surface pH maxima gradually diminished in one of the microcosms and completely dissipated in the other (Fig. S7). Compared with day 43, Ca^{2+}/Na^{+} distributions did not significantly change with an enrichment peak of 0.033 centered at 1–2 cm depth, and much higher Ca^{2+}/Na^{+} ratios in the deep sediment layer (3–5 cm) (Fig. 4B). However, Mg^{2+}/Na^{+} increased in the surface sediment layer compared with oxygenated boundary conditions as of day 43 (0.109 vs. 0.112) (Fig. 6). Thermodynamic calculations indicated that Mg-calcite (5–20 mol% Mg) in the top-most layer became less saturated ($\Omega = \sim 1$) after 6 h of overlying water anoxia, and the saturation state minimum became less obvious in the anodic zone (Fig. 4). Numerical modelling of porewater Ca^{2+} and Mg^{2+} distributions during a 6-h anoxic period showed that diffusion alone could produce only minor variation at depth over such a short time (Figs. 4 & 6, day 43). After the 6-h anoxic period on day 106, phosphate distributions and R-ΣPO_4^{3-} only changed slightly from day 43, when the electrogenic colonization was active (Fig. 7).

4. Discussion

4.1. Electrogenic metabolism in Fe, Mn-depleted carbonate deposits

The importance of redox reactive metals involved in long-distance electrogenic metabolism has still not been clarified even though their biogeochemical cycling can clearly interact with cable bacteria in multiple ways (Risgaard-Petersen et al., 2012; Sulu-Gambari et al., 2016a; Sulu-Gambari et al., 2016b). Fe and Mn are depleted in Florida Bay sediments, providing a natural experiment for electrogenic activity at low Fe and Mn concentrations. In our study, the surface 5 cm sediment porewater samples were analyzed for Fe and Mn in order to determine their possible role in pH dynamics, however, both dissolved Fe and Mn were below the detection limit of the analytical methods (< 1–2 μM using Ferrozine, formaldoxime methods (Goto et al., 1962; Stookey, 1970; Zhu and Aller, 2012). Sediment surface element composition was also analyzed under SEM-EDS, confirming a very low content of Fe (Fig. S15) consistent with reported ranges from Florida Bay (Caccia et al., 2003). Cable bacteria activity was confirmed by the characteristic pH distributions, the presence of distinctive multicellular bacteria filaments, consumption of H_2S at depths well-below the oxic zone, the inhibition of characteristic reaction patterns by permeable physical barriers (filter paper), and inhibition of activity by overlying water deoxygenation. These findings demonstrate that sustained cable bacteria dissimilatory activity does not necessarily require solid phase sulfides in the ambient sediment if a sufficient dissolved sulfide source is available. Unlike lithogenic sediments, where Fe and Mn are abundant and cable bacteria can take advantage of both dissolved and an often large pool of solid phase sulfides after dissolution (Nielsen and Risgaard-Petersen, 2015), in carbonate deposits, cable bacteria can only access dissolved H_2S. In recent studies, Müller et al. (2020) argued that S disproportionation by groundwater cable bacteria was promoted by Fe scavenging of dissolved sulfide and formation of elemental sulfur intermediate. Sulfur disproportionation coupled to redox-reactive metals is unlikely to have been an important pathway in carbonate muds from Florida Bay due to the very low concentrations of Fe (Fig.S15) (Caccia et al., 2003; Ku et al., 1999).

In addition to pH patterns, the H_2S dynamics are another strong piece of evidence for the existence of cable bacteria activity. Three primary H_2S consumption pathways are possible in Florida Bay sediments: (1) abiogenic or chemoautotrophic oxidation by O_2, (2) oxidation using NO_3^-, and (3) electrogenic sulfide oxidation. Oxygen and

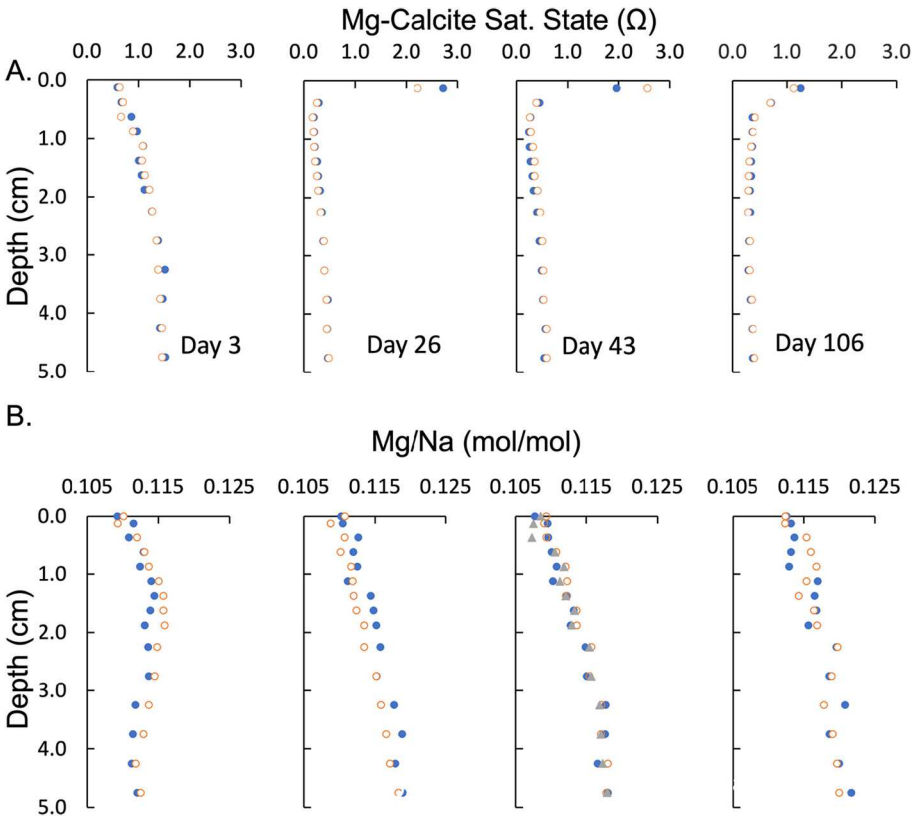

Fig. 6. Mg-calcite saturation state and Mg^{2+}/Na^{+} distribution dynamics in series II experiments. A. Mg-calcite (20 mol% Mg) saturation state on day 3, 26, 43, and 106. The day 106 profile was measured after 6 h of overlying water anoxia. The sediment oxic layer became Mg-calcite supersaturated along with the development of cable bacteria from day 3 to 43. A Ω minimum was evident in the 0.5–1 cm depth. After 6 h of overlying water anoxia, Mg-calcite in the sediment surface became less saturated, and the Ω minimum disappeared. B. Mg^{2+}/Na^{+} distribution dynamics. Mg^{2+} increased with depth during incubation period for all the measurements and no time dependent patterns were observed. After 6 h of anoxia, Mg^{2+}/Na^{+} increased in the surface sediment suggesting hi-Mg-calcite dissolution occurred. Color coding (blue and orange) shows results from duplicate microcosms. The gray triangles in day 43 profile are the modeled average Mg^{2+}/Na^{+} ratios as it would appear if the production/consumption of Mg^{2+} ceased immediately after anoxic exposure for 6 h and then diffusion was the only process controlling its distribution. (For interpretation of the references to color in this figure legend, the reader is referred to the web version of this article.)

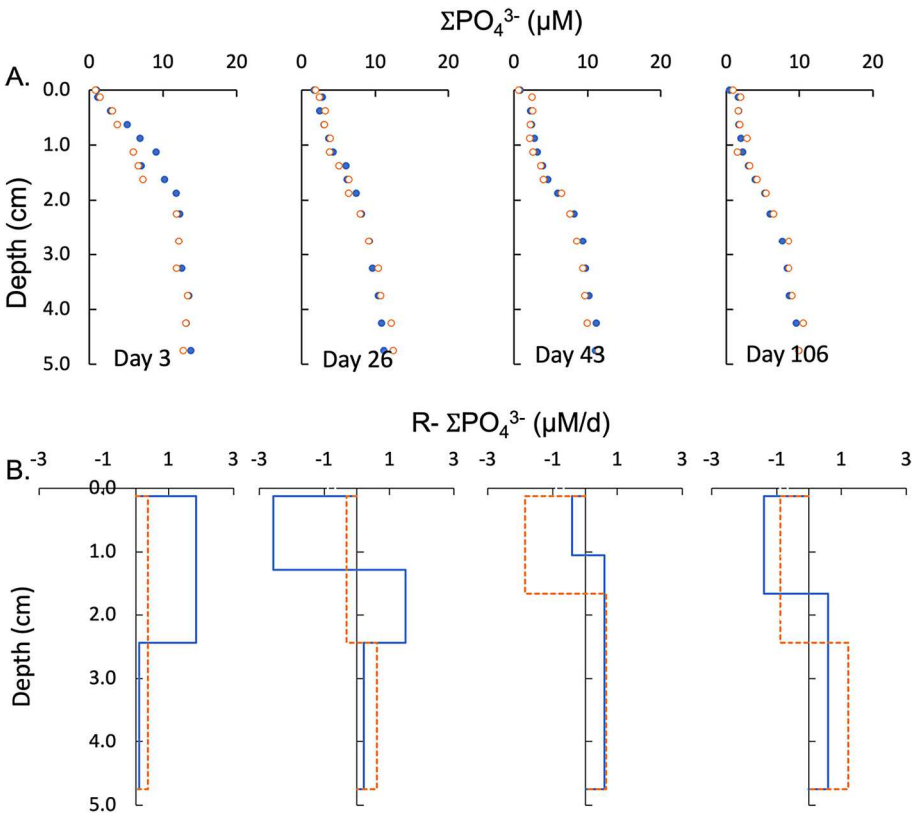

Fig. 7. Phosphate distribution dynamics on day 3, 26, 43, and 106 and the associated ΣPO_4^{3-} reaction rates (R-ΣPO_4^{3-}) in series II experiments. The day 106 profile was measured after 6 h of anoxia. A. From day 26 to 43, the concave shape of phosphate concentrations above the 2 cm depth overlapped with the electrogenic reaction zone. B. R-PO_4^{3-} estimation shows that a distinct phosphate consumption zone appeared above 2 cm depth. Color coding shows results from duplicate microcosms.

nitrate penetration depths are both shallow (oxygen: 2 mm; nitrate: 5 mm, Fig. S8), and with our modelling are not separately distinguished. R-H_2S cannot estimate the reaction rates in the oxygen and nitrate penetration zone due to nondetectable H_2S, however, there is no doubt that non-electrogenic sulfide consumption dominated the overall sulfide removal in the surface sediment before cable bacteria colonization. When characteristic electrogenic pH patterns became evident, subsurface consumption of sulfide also became detectable, resulting in a transition from sulfide consumption exclusively near the sediment-water interface to dominant subsurface anodic zones (Fig. 1B). The apparent presence of two H_2S consumption zones suggest a co-existence of non-electrogenic chemoautotrophic (or abiogenic) oxidation near the sediment-water interface and subsurface electrogenic oxidation pathways at least during the transition period (day 26). However, because of the low resolution of reaction rates in the upper ~1 cm, it is possible that H_2S consumption near the interface is also due to cable bacteria after day 26. The upper boundary of the deep consumption zones and H_2S detectable depths deepened progressively (Fig. 1&2A), consistent with the deepening of Ca^{2+} enrichment peaks (carbonate dissolution) (Fig. 4B) and the indication that cable bacteria clustered at different depths during initial developmental stages. The eventual decreasing magnitude of the sulfide consumption rate, R-H_2S, in the electrogenic anodic zone and thus current density with time in one of the duplicate microcosms (Table 2 and Fig. S1) indicates the eventual decline of cable bacteria activity, consistent with the dissipating sediment surface pH maxima and cessation of anodic zone expansion (Fig. 2B & S4).

4.2. Anoxic sediment pH dynamics

Along with sediment surface pH elevation, there is often a pH minimum zone detected in association with the anodic reaction (Nielsen et al., 2010). However, the pH minimum signal was not strongly expressed in this study (see also Yin et al., 2021b). Others have reported similar sediment surface pH maxima without obvious subsurface pH minima (Burdorf et al., 2017; Malkin et al., 2017). In carbonate muds of Florida Bay, total alkalinity often exceeds 5 mM at depths >1 cm (Fig. S5). The high total alkalinity reflects both high anaerobic C_{org} remineralization rates, typically found within seagrass beds and areas nearby, and the dissolution of the carbonate matrix, which directly buffers acid, making it more difficult to detect acidification (pH decrease) caused by cable bacteria activity. We recently also concluded that the detection of electrogenic pH minima can be hampered by the fast proton diffusion rate (heavily dependent on sediment porosity) in anoxic sediments (Yin et al., 2021b).

4.3. Cable bacteria distribution patterns and development of electrogenic activity

The discovery of distinctive filaments immediately after microcosms were set up confirms that the cable bacteria were originally present in carbonate deposits (Fig. 3a), further expanding their known distribution across a range of natural environments (Burdorf et al., 2017). The density of cable bacteria filaments reported in carbonate sediment (Table 2) is comparable with densities reported in other studies from various sediment types, although in the higher range (Hermans et al., 2020; Malkin et al., 2017; Schauer et al., 2014). For example, Schauer et al. (2014) reported a maximum density value of 2380 m/cm^2 in the top 3 cm of lithogenic marine sediment, and the maximum number we observed is 2840 m/cm^2, in the upper 5 cm sediment (i.e., 1700 m/cm^2 in the top 3 cm sediment). Because of our methodology, it is possible that we have counted filamentous bacteria that are not genetically true cable bacteria; however, it is clear from biogeochemical reaction patterns that

they function as such. Unexpectedly, cable bacteria filaments were also found in abundance in the sediment at depth below the filter barrier in series III experiments (Fig. S9). Those cable bacteria were unable to carry out electrogenic reactions coupled to O_2 reduction, but they might conduct other modes of metabolism or stay dormant in the laboratory settings.

Given the mobility of cable bacteria (Bjerg et al., 2016), and the requirement for stable redox domains, cable bacteria filaments can orient to access the highly favorable redox conditions present in laboratory manipulations (Scholz et al., 2021; Scholz et al., 2019; Yin et al., 2021a). In our experiments, the initial increase in cable bacteria cell abundance occurred mainly in the anodic zone, with little variability in filamentous cell abundance in the cathodic zone. The observation from a parallel set of microcosm experiments (Fig. 1 & S1) was discussed in detail in Yin et al. (2021b). It is consistent with a location-specific role in energy conservation in the multicellular cable bacteria filaments (Geerlings et al., 2020). The spherical or oval-shaped appearance of a single nucleoid region in each cell within the sediment oxic layer (Fig. 3C, also observed by Geerlings et al. (2021)) indicates no division in the cathodic end. Clearly, when cable bacteria are present in sediments, they dominate as filamentous morphologies under stable conditions such as in the laboratory. However, the exact expression of their activity in nature must vary substantially and may mimic laboratory patterns only under similarly stable conditions.

The dynamics of cable bacteria growth and demise, as reflected in electrogenic pH patterns, can vary substantially in carbonate sediment, even under ideal, stable laboratory conditions. In series I experiments, sediment surface pH maxima were detected after 9 days yet completely disappeared on day 27 (Fig. S11). In series II experiments, electrogenic activity was detected before day 26, but diminished slightly in one of the duplicate microcosms after 106 days (Fig. S1). The differences in results may have been caused by sediment handling (e.g., the time delay between sample collection and experiment start) and sediment variations between years. The differences between cable bacteria dynamics in otherwise similar sediments could have also come from seasonal differences in the natural condition of the cable bacteria at the time of collection (Seitaj et al., 2015) and/or differences in the production flux of dissolved sulfide (H_2S production rates) (Yin et al., 2021b). In any case, variation in the development times of cable bacteria filaments demonstrates that there is no single timescale that defines cable bacteria establishment and that a wide time range (between 7 and 24 days in the current study) is possible. Others have reported that ~7–10 days is common for the establishment of filament growth following stabilization of redox conditions (Burdorf et al., 2017; Rao et al., 2016).

The reason for the decline of cable bacteria activity during incubation is not obvious in the present research. It has been argued in previous studies of lithogenic sediments that the exhaustion of sulfide, potentially FeS, might be the cause (Rao et al., 2016; Schauer et al., 2014). In the present study, there was sufficient H_2S (~100 μM; although the supply of sulfide from deep sediment decreased with time (Fig. S4), no grazers (based on microscopic examination for meiofauna), and no macrofaunal bioturbators in series I microcosm experiments. Despite what appears to be favorable conditions, both pH and H_2S dynamics suggest the collapse of electrogenic sulfide oxidation on day 27 in series I (Fig. S10). There were juvenile bioturbators in experiment series II, however, they were only believed to have a localized negative impact (Yin et al., 2021a). There was an indication by day 106 of a decline in cable bacteria activity as indicated by the cessation in the deepening of the H_2S anodic consumption front (Fig. 2B), a decrease in the sediment surface pH, and decreased electrogenic H_2S consumption rates (Table 2, Fig. S1B), but activity remained detectable. Interestingly, when long distance electron transport metabolism started to collapse, we did not find that cable bacteria cell abundance decreased (Table 1). This lack of a numerical response suggests that their metabolic mode was changing, consistent with the hypothesis that these organisms are metabolic opportunists (Aller et al., 2019). Recent studies have found that in lithogenic deposits, mineral precipitates in the surface oxic layers coated the cathodic ends of the bacteria (Geerlings et al., 2019). Such encrustations might create a diffusion barrier, hampering filament mobility and flexibility, and impeding their cable-based metabolism. We found an increased abundance of cells in the sediment oxic layer at the end of the incubation period (Fig. 1, s1 and S10). We infer that this increase is a compensatory response to carbonate mineral encrustation. Ultimately, the self-limiting deposition of minerals might cause a decline in the advantages of the cable morphology as a mode of respiration.

4.4. Cable bacteria activity impacts carbonate mineral distributions

Elevated pH in the oxic layer and pH minima in the subsurface anodic zone promote carbonate precipitation and dissolution in carbonate sediments, respectively. Similar carbonate dynamics associated with electrogenic reaction have been documented in lithogenic deposits (Rao et al., 2016; Risgaard-Petersen et al., 2012). Porewater Ca^{2+} enrichment in the anodic zone of electrogenic reaction (cm-scale depth) demonstrates that carbonate mineral cycling can be closely coupled to cable bacteria activity in Florida Bay (Fig. 4). When electrogenic sulfide oxidation was inhibited by a permeable physical barrier in the control microcosm (inferred from the lack of electrogenic pH fingerprint), such a readily distinguishable porewater Ca^{2+} distribution was absent (Fig. 5). When electrogenic sulfide oxidation is active, thermodynamic saturation state calculations show that aragonite and hi-Mg-calcites are supersaturated in the topmost sediment layer and undersaturated with a minimum Ω in the suboxic/sulfidic layer (Fig. 4A & 6A). No porewater samples were available between day 43 and 106 in the current study, but we assume that sediment Ca^{2+}, Mg^{2+} and the associated mineral saturation state distributions did not change significantly from day 43 to 106 when the microcosms were subjected to a 6-h period with deoxygenated overlying water. The following discussion is based on that assumption.

The carbonate saturation state in the topmost sediment layer decreased on day 106 after the 6-h period of anoxia, suggesting the decline of cable bacteria activity without abundant ambient electron acceptors (i.e., O_2) (Fig. S7). The response of Ca^{2+} profiles after the cessation of electrogenic reactions is slow compared with the decline of the pH fingerprints, as reflected by the sustained Ca^{2+} production peaks in the cable bacteria anodic reaction zone (Fig. 4 & S7). Similar distributions of Ca^{2+} were observed on day 27 in series I after the complete disappearance of sediment surface pH maxima signals (Fig. S14). The slow response of Ca^{2+} and Mg^{2+} profiles could be caused by the slow diffusion rates of Ca^{2+} and Mg^{2+} in the anoxic deeper sediment (lower porosity) and slow carbonate dissolution kinetics. Our model simulation, where production/consumption ceased immediately and diffusion was the only process affecting Ca^{2+} and Mg^{2+} distributions, showed that only minor changes could be expected during a 6-h anoxic period (Fig. 4B & 6B). Thus, to relax an existing profile of centimeter scale would take on the order of a day, longer than the measurement period.

Hi-Mg-calcite precipitation (>5 mol% Mg) was promoted in the surface pH maximum zones of lithogenic sediments in other studies (Risgaard-Petersen et al., 2012). Here we find that there was dissolved Mg^{2+} depletion in the surface sediment when cable bacteria were active, strongly suggesting the precipitation of hi-Mg-calcite (Fig. 6B, day 43). Thermodynamic calculations also confirmed that Mg-calcite (5–20 mol % Mg) was supersaturated in the topmost layer. However, Mg^{2+} behaved differently from Ca^{2+} in the cable bacteria anodic reaction zone, thus cable bacteria activity may have different effects on carbonate mineral cycling (lo-, hi-Mg-calcite, and aragonite), at least in this study. The absence of Mg^{2+} enrichment peaks in the anodic zone of our carbonate sediments indicates that Mg-calcite re-precipitation occurred simultaneously with dissolution or that the dissolution sources are dominated by aragonite or lo-Mg-calcite. Aragonite is more soluble than lo-Mg-calcite and is present as fine needles (5 μm in length and 0.1–0.5 μm in width) produced by benthic calcareous macroalgae like *Halimeda*; these needles are highly susceptible to dissolution (Morse and

Mackenzie, 1990; Peach et al., 2017). Although we did not measure them in this study, Sr^{2+} and F^{-} enrichments in Florida Bay porewater are consistent with such a source near the sediment-water interface (Rude and Aller, 1991). After 6 h of anoxia, it appears that the recently formed authigenic hi-Mg-Calcite (presumably) quickly dissolved, causing higher Mg^{2+} concentrations in the surface sediment (Fig. 6B). These reaction patterns and rapid responses to overlying water O_2 show that cable bacteria must be considered as a component of highly dynamic mineral cycling in carbonate deposits (e.g., Walter and Burton, 1990).

4.5. Effect of cable bacteria on P cycling in carbonate deposits

The concave-shape curve of phosphate distributions in the top 2 cm of sediment indicates phosphate consumption occurred in the electrogenic reaction zone (Fig. 7A). Reaction rate simulations support phosphate consumption in that depth interval (Fig. 7B). Cable bacteria are known to strongly affect the cycling of P in lithogenic sediments because of both the association of ΣPO_4^{3-} with Fe- and Mn-oxides formed in the cable bacteria cathodic reaction zone and intracellular accumulation of polyphosphates (Geerlings et al., 2019; Sulu-Gambari et al., 2016b). Fe- and Mn-oxides are depleted in Florida Bay compared with lithogenic sediments (Caccia et al., 2003), and thus the coupling of ΣPO_4^{3-} to Fe- and Mn-oxide cycling by cable bacteria is not important in carbonate deposits. However, ΣPO_4^{3-} is also strongly adsorbed by carbonate minerals and can be incorporated during the formation of authigenic minerals such as carbonate fluorapatites, which could also explain the overall low concentrations of ΣPO_4^{3-} in series II (Rude and Aller, 1991; Tunesi et al., 1999). Such reactions are almost certainly involved in the consumption of ΣPO_4^{3-} in the surface zones of the microcosms. However, the absence of measurable elevation peaks of ΣPO_4^{3-} and negative R-ΣPO_4^{3-} simulations contrast with Ca^{2+} enrichments and positive R-Ca^{2+} predictions in the anodic zone (0.5–1.5 cm depth) suggesting that the release of phosphate during carbonate dissolution was compensated by intracellular assimilation or re-adsorption on mineral surfaces (Figs. 4 & 7). Based on cable bacteria filament abundance, we estimate that cable bacteria intracellular phosphate incorporation has the potential to decrease porewater phosphate by 50–900 μM (35–650 μM without considering intracellular polyphosphate granules) in the top 1.5 cm where phosphate consumption was observed (Fig. 7, day 43). This calculation suggests that cable bacteria biomass could be a major sink for P in addition to simultaneously promoting dissolved P production in FLB deposits. In contrast, Sulu-Gambari et al. (2016b) argued that intracellular phosphate incorporation was negligible compared with Fe-oxide-bound-P. These different inferences could be partially due to the different P/C ratios (0.072 vs. 0.013) used in the estimations. Porewater phosphate would potentially decrease 9–163 or 6–118 μM (without considering intracellular polyphosphate granules) if the P/C ratio from Sulu-Gambari et al. (2016b) was used.

P is a primary limiting nutrient for seagrasses in the carbonate sediments (Fourqurean et al., 1992). Because seagrasses export O_2 into their rhizosphere, it promotes subsurface carbonate dissolution (Burdige et al., 2008). It seems likely that cable bacteria associate closely with such physically stable, oxygenated seagrass root systems and increase nitrogen availability for plants (Kessler et al., 2019; Kjeldsen et al., 2019; Martin et al., 2019; Scholz et al., 2021; Scholz et al., 2019). They may also promote carbonate dissolution and mobilization of P in microenvironments that could be available to seagrasses, as well as simultaneously decreasing the flux of toxic H_2S to roots. The relative fate of mobilized P with respect to uptake by cable bacteria and/or seagrasses however remains an open question, but clearly one of importance for understanding P cycling in seagrass-dominated systems such as Florida Bay.

5. Summary

It is clear that cable bacteria can develop and demonstrate strong electrogenic activity without apparent redox cycling of Fe and Mn. The spontaneous decline in signals of cable bacteria activity despite the continued presence of filaments and sustained sulfide supply at the end of the laboratory incubation period suggests that the abundance of cable bacteria alone need not relate directly to the effects of their activity on sediment early diagenesis. The limited amount of extracellular Fe in carbonate deposits also implies that a hypothesized sulfur disproportionation pathway mediated with redox sensitive metals in groundwater is an unnecessary reaction step in these environments. During cable bacteria colonization, non-electrogenic (abiogenic or chemoautotrophic) H_2S oxidation near the sediment-water interface apparently took place simultaneously with electrogenic H_2S oxidation at depth.

Dissolution of solid phase sulfides is not a component of electrogenic activity in carbonates, simplifying diagenetic reaction pathways and possible additional interactions of cable bacteria with redox sensitive metals. The geochemical impacts of cable bacteria were evaluated in Fe and Mn depleted carbonate sediments. Cable bacteria activity can strongly impact carbonate mineral distributions. Subsurface release of P during carbonate dissolution and intracellular P assimilation by cable bacteria may play important roles in controlling P availability and P cycling in carbonate deposits, particularly with respect to seagrass rhizospheres. Although the potential of cable bacteria to impact a wide range of diagenetic reactions in carbonate deposits was clearly demonstrated, the exact realization of their activities under field conditions remains to be determined.

Data availability statement

The data that support the findings of this study are openly available at https://www.doi.org/10.5281/zenodo.7076315 and through the NSF Biological and Chemical Oceanography Data Management Office.

Declaration of Competing Interest

None.

Acknowledgements

We thank W. Cong, Z. Qi, M. Wheeler, and C. Heilbrun for assistance in the field and laboratory, and D. Black for aid with ICP-OES measurements. A. Kessler (Monash University), S. Malkin, N. Risgaard-Petersen, F. Meysman, and anonymous reviewers provided constructive, critical comments. This work is supported by NSF OCE 1737749 and NSF OCE 1332418.

Appendix A. Supplementary data

Supplementary data to this article can be found online at https://doi.org/10.1016/j.marchem.2022.104176.

References

Aller, R.C., et al., 2019. Worm tubes as conduits for the electrogenic microbial grid in marine sediments. Sci. Adv. 5 (7), eaaw3651.
Berg, P., Risgaard-Petersen, N., Rysgaard, S., 1998. Interpretation of measured concentration profiles in sediment pore water. Limnol. Oceanogr. 43 (7), 1500–1510.
Bjerg, J.T., Damgaard, L.R., Holm, S.A., Schramm, A., Nielsen, L.P., 2016. Motility of electric cable bacteria. Appl. Environ. Microbiol. 82, 3816–3821. https://doi.org/10.1128/AEM.01038-16.
Boudreau, B.P., 1997. Diagenetic Models and their Implementation, 505. Springer, Berlin.
Burdige, D.J., Zimmerman, R.C., Hu, X., 2008. Rates of carbonate dissolution in permeable sediments estimated from pore-water profiles: the role of sea grasses. Limnol. Oceanogr. 53 (2), 549–565.
Burdorf, L.D., et al., 2017. Long-distance electron transport occurs globally in marine sediments. Biogeosciences 14 (3), 683.
Caccia, V.G., Millero, F.J., Palanques, A., 2003. The distribution of trace metals in Florida bay sediments. Mar. Pollut. Bull. 46 (11), 1420–1433.

Cornelissen, R., et al., 2018. The cell envelope structure of cable bacteria. Front. Microbiol. 9, 3044.
Fagerbakke, K.M., Heldal, M., Norland, S., 1996. Content of carbon, nitrogen, oxygen, sulfur and phosphorus in native aquatic and cultured bacteria. Aquat. Microb. Ecol. 10 (1), 15–27.
Fourqurean, J.W., Zieman, J.C., Powell, G.V., 1992. Phosphorus limitation of primary production in Florida bay: evidence from C: N: P ratios of the dominant seagrass Thalassia testudinum. Limnol. Oceanogr. 37 (1), 162–171.
Froelich, P.N., et al., 1979. Early oxidation of organic matter in pelagic sediments of the eastern equatorial Atlantic: suboxic diagenesis. Geochim. Cosmochim. Acta 43 (7), 1075–1090.
Geerlings, N., Zetsche, E.-M., Hidalgo-Martinez, S., Middelburg, J.J., Meysman, F.J., 2019. Mineral formation induced by cable bacteria performing long-distance electron transport in marine sediments. Biogeosciences 16 (3), 811–829.
Geerlings, N.M., et al., 2020. Division of labor and growth during electrical cooperation in multicellular cable bacteria. Proc. Natl. Acad. Sci. 117 (10), 5478–5485.
Geerlings, N.M., et al., 2021. Cell cycle, filament growth and synchronized cell division in multicellular cable bacteria. Front. Microbiol. 12, 46.
Ginsburg, R., 1972. South Flordia Carbonate Sediments: Sedimentation II, 72. University of Miami.
Goto, K., Komatsu, T., Furukawa, T., 1962. Rapid colorimetric determination of manganese in waters containing iron: a modification of the formaldoxime method. Anal. Chim. Acta 27, 331–334.
Hermans, M., Risgaard-Petersen, N., Meysman, F.J., Slomp, C.P., 2020. Biogeochemical impact of cable bacteria on coastal Black Sea sediment. Biogeosciences 17 (23), 5919–5938.
Hermans, M., et al., 2021. Coupled dynamics of iron, manganese, and phosphorus in brackish coastal sediments populated by cable bacteria. Limnol. Oceanogr. 66 (7), 2611–2631.
Jiang, Z., et al., 2018. In vitro single-cell dissection revealing the interior structure of cable bacteria. Proc. Natl. Acad. Sci. 115 (34), 8517–8522.
Kessler, A.J., et al., 2019. Cable bacteria promote DNRA through iron sulfide dissolution. Limnol. Oceanogr. 64 (3), 1228–1238.
Kjeldsen, K.U., et al., 2019. On the evolution and physiology of cable bacteria. Proc. Natl. Acad. Sci. 116 (38), 19116–19125.
Ku, T., Walter, L., Coleman, M., Blake, R., Martini, A., 1999. Coupling between sulfur recycling and syndepositional carbonate dissolution: evidence from oxygen and sulfur isotope composition of pore water sulfate, South Florida platform, USA. Geochim. Cosmochim. Acta 63 (17), 2529–2546.
Larsen, S., Nielsen, L.P., Schramm, A., 2015. Cable bacteria associated with long-distance electron transport in New England salt marsh sediment. Environ. Microbiol. Rep. 7 (2), 175–179.
Lee, S.-K., Okura, I., 1997. Photostable optical oxygen sensing material: platinum tetrakis (pentafluorophenyl) porphyrin immobilized in polystyrene. Anal. Commun. 34 (6), 185–188.
Loferer-Krößbacher, M., Klima, J., Psenner, R., 1998. Determination of bacterial cell dry mass by transmission electron microscopy and densitometric image analysis. Appl. Environ. Microbiol. 64 (2), 688–694.
Malkin, S.Y., et al., 2014. Natural occurrence of microbial Sulphur oxidation by long-range electron transport in the seafloor. ISME J. 8 (9), 1843–1854.
Malkin, S.Y., et al., 2017. Electrogenic sulfur oxidation by cable bacteria in bivalve reef sediments. Front. Mar. Sci. 4, 28.
Manz, W., Amann, R., Ludwig, W., Wagner, M., Schleifer, K.-H., 1992. Phylogenetic oligodeoxynucleotide probes for the major subclasses of proteobacteria: problems and solutions. Syst. Appl. Microbiol. 15 (4), 593–600.
Martin, B.C., et al., 2019. Oxygen loss from seagrass roots coincides with colonisation of sulphide-oxidising cable bacteria and reduces sulphide stress. The ISME Journal 13 (3), 707.
Marzocchi, U., et al., 2014. Electric coupling between distant nitrate reduction and sulfide oxidation in marine sediment. ISME J. 8 (8), 1682–1690.
Meysman, F.J., 2018. Cable bacteria take a new breath using long-distance electricity. Trends Microbiol. 26 (5), 411–422.
Meysman, F.J., Risgaard-Petersen, N., Malkin, S.Y., Nielsen, L.P., 2015. The geochemical fingerprint of microbial long-distance electron transport in the seafloor. Geochim. Cosmochim. Acta 152, 122–142.
Meysman, F.J., et al., 2019. A highly conductive fibre network enables centimetre-scale electron transport in multicellular cable bacteria. Nat. Commun. 10 (1), 1–8.
Millero, F.J., 1979. The thermodynamics of the carbonate system in seawater. Geochim. Cosmochim. Acta 43 (10), 1651–1661.
Miranda, K.M., Espey, M.G., Wink, D.A., 2001. A rapid, simple spectrophotometric method for simultaneous detection of nitrate and nitrite. Nitric Oxide 5 (1), 62–71.
Morse, J.W., Mackenzie, F.T., 1990. Geochemistry of Sedimentary Carbonates. Elsevier.
Morse, J.W., Andersson, A.J., Mackenzie, F.T., 2006. Initial responses of carbonate-rich shelf sediments to rising atmospheric pCO2 and “ocean acidification”: role of high Mg-calcites. Geochim. Cosmochim. Acta 70 (23), 5814–5830.
Müller, H., et al., 2016. Long-distance electron transfer by cable bacteria in aquifer sediments. The ISME Journal 10 (8), 2010–2019.
Müller, H., Marozava, S., Probst, A.J., Meckenstock, R.U., 2020. Groundwater cable bacteria conserve energy by sulfur disproportionation. The ISME Journal 14 (2), 623–634.
Murphy, J., Riley, J.P., 1962. A modified single solution method for the determination of phosphate in natural waters. Anal. Chim. Acta 27, 31–36.
Nielsen, L.P., Risgaard-Petersen, N., 2015. Rethinking sediment biogeochemistry after the discovery of electric currents. Annu. Rev. Mar. Sci. 7, 425–442.
Nielsen, L.P., Risgaard-Petersen, N., Fossing, H., Christensen, P.B., Sayama, M., 2010. Electric currents couple spatially separated biogeochemical processes in marine sediment. Nature 463 (7284), 1071–1074.
Peach, K.E., Koch, M.S., Blackwelder, P.L., Manfrino, C., 2017. Calcification and photophysiology responses to elevated pCO2 in six Halimeda species from contrasting irradiance environments on little Cayman Island reefs. J. Exp. Mar. Biol. Ecol. 486, 114–126.
Pfeffer, C., et al., 2012. Filamentous bacteria transport electrons over centimetre distances. Nature 491 (7423), 218–221.
Rao, A.M., Malkin, S.Y., Hidalgo-Martinez, S., Meysman, F.J., 2016. The impact of electrogenic sulfide oxidation on elemental cycling and solute fluxes in coastal sediment. Geochim. Cosmochim. Acta 172, 265–286.
Reimers, C.E., Li, C., Graw, M.F., Schrader, P.S., Wolf, M., 2017. The identification of cable bacteria attached to the anode of a benthic microbial fuel cell: evidence of long distance extracellular electron transport to electrodes. Front. Microbiol. 8, 2055.
Risgaard-Petersen, N., Revil, A., Meister, P., Nielsen, L.P., 2012. Sulfur, iron-, and calcium cycling associated with natural electric currents running through marine sediment. Geochim. Cosmochim. Acta 92, 1–13.
Risgaard-Petersen, N., et al., 2015. Cable bacteria in freshwater sediments. Appl. Environ. Microbiol. 81 (17), 6003–6011.
Robbins, L., Hansen, M., Kleypas, J., Meylan, S., 2010. CO2calc: A User-Friendly Seawater Carbon Calculator for Windows, Mac OS X, and iOS (iPhone). 2331–1258. US Geological Survey.
Rude, P.D., Aller, R.C., 1991. Fluorine mobility during early diagenesis of carbonate sediment: an indicator of mineral transformations. Geochim. Cosmochim. Acta 55 (9), 2491–2509.
Sarazin, G., Michard, G., Prevot, F., 1999. A rapid and accurate spectroscopic method for alkalinity measurements in sea water samples. Water Res. 33 (1), 290–294.
Schauer, R., et al., 2014. Succession of cable bacteria and electric currents in marine sediment. The ISME Journal 8 (6), 1314.
Scholz, V.V., Müller, H., Koren, K., Nielsen, L.P., Meckenstock, R.U., 2019. The rhizosphere of aquatic plants is a habitat for cable bacteria. FEMS Microbiol. Ecol. 95 (6), fiz062.
Scholz, V.V., et al., 2021. Cable bacteria at oxygen-releasing roots of aquatic plants: a widespread and diverse plant-microbe association. New Phytol. 232 (5), 2138–2151.
Seitaj, D., et al., 2015. Cable bacteria generate a firewall against euxinia in seasonally hypoxic basins. Proc. Natl. Acad. Sci. 112 (43), 13278–13283.
Stabenau, E., Kotun, K., 2012. Salinity and Hydrology of Florida Bay: Status and Trends 1990–2009. National Park Service, Everglades National Park, South Florida Natural Resources Center, Homestead, FL. Status and Trends Report SFNRC Tech-nical Series 2012:1(2012:1), 39 pp.
Stookey, L.L., 1970. Ferrozine—a new spectrophotometric reagent for iron. Anal. Chem. 42 (7), 779–781.
Sulu-Gambari, F., et al., 2016a. Impact of cable bacteria on sedimentary iron and manganese dynamics in a seasonally-hypoxic marine basin. Geochim. Cosmochim. Acta 192, 49–69.
Sulu-Gambari, F., et al., 2016b. Cable bacteria control iron–phosphorus dynamics in sediments of a coastal hypoxic basin. Environ. Sci. Technol. 50 (3), 1227–1233.
Thamdrup, B., 2000. Bacterial Manganese and Iron Reduction in Aquatic Sediments, Advances in Microbial Ecology. Springer, pp. 41–84.
Trojan, D., et al., 2016. A taxonomic framework for cable bacteria and proposal of the candidate genera Electrothrix and Electronema. Syst. Appl. Microbiol. 39 (5), 297–306.
Tunesi, S., Poggi, V., Gessa, C., 1999. Phosphate adsorption and precipitation in calcareous soils: the role of calcium ions in solution and carbonate minerals. Nutr. Cycl. Agroecosyst. 53 (3), 219–227.
Ullman, W.J., Aller, R.C., 1985. The geochemistry of iodine in near-shore carbonate sediments. Geochim. Cosmochim. Acta 49 (4), 967–978.
van de Velde, S., et al., 2016. The impact of electrogenic sulfur oxidation on the biogeochemistry of coastal sediments: a field study. Geochim. Cosmochim. Acta 194, 211–232.
van de Velde, S., Callebaut, I., Gao, Y., Meysman, F.J., 2017. Impact of electrogenic sulfur oxidation on trace metal cycling in a coastal sediment. Chem. Geol. 452, 9–23.
Walter, L.M., Burton, E.A., 1990. Dissolution of recent platform carbonate sediments in marine pore fluids. Am. J. Sci. 290 (6), 601–643.
Wanless, H.R., Tagett, M.G., 1989. Origin, growth and evolution of carbonate mudbanks in Florida bay. Bull. Mar. Sci. 44 (1), 454–489.
Xu, X., Huo, S., Zhang, H., Li, X., Wu, F., 2021. Identification of cable bacteria and its biogeochemical impact on sulfur in freshwater sediments from the Wenyu River. Sci. Total Environ. 769, 144541.
Yin, H., Zhu, Q., Aller, R.C., 2017. An irreversible planar optical sensor for multi-dimensional measurements of sedimentary H2S. Mar. Chem. 195, 143–152.
Yin, H., Aller, R., Zhu, Q., Aller, J., 2021a. Biogenic structures and cable bacteria interactions: Redox domain residence times and the generation of complex pH distributions. Mar. Ecol. Prog. Ser. 669, 51–63 (Accepted).
Yin, H., Aller, R.C., Zhu, Q., Aller, J.Y., 2021b. The dynamics of cable bacteria colonization in surface sediments: a 2D view. Sci. Rep. 11, 7167.
Zhu, Q., Aller, R.C., 2012. Two-dimensional dissolved ferrous iron distributions in marine sediments as revealed by a novel planar optical sensor. Mar. Chem. 136, 14–23.
Zhu, Q., Aller, R.C., Fan, Y., 2006. Two-dimensional pH distributions and dynamics in bioturbated marine sediments. Geochim. Cosmochim. Acta 70 (19), 4933–4949.